Bacterial Shape and ActA Distribution Affect Initiation of *Listeria monocytogenes* Actin-Based Motility

Susanne M. Rafelski* and Julie A. Theriot*†
*Department of Biochemistry and †Department of Microbiology and Immunology, Stanford University Medical Center, Stanford, California 94305-5307

ABSTRACT We have examined the process by which the intracellular bacterial pathogen *Listeria monocytogenes* initiates actin-based motility and determined the contribution of the variable surface distribution of the ActA protein to initiation and steady-state movement. To directly correlate ActA distributions to actin dynamics and motility of live bacteria, ActA was fused to a monomeric red fluorescent protein (mRFP1). Actin comet tail formation and steady-state bacterial movement rates both depended on ActA distribution, which in turn was tightly coupled to the bacterial cell cycle. Motility initiation was found to be a highly complex, multistep process for bacteria, in contrast to the simple symmetry breaking previously observed for ActA-coated spherical beads. F-actin initially accumulated along the sides of the bacterium and then slowly migrated to the bacterial pole expressing the highest density of ActA as a tail formed. Early movement was highly unstable with extreme changes in speed and frequent stops. Over time, saltatory motility and sensitivity to the immediate environment decreased as bacterial movement became robust at a constant steady-state speed.

INTRODUCTION

Listeria monocytogenes is a Gram-positive facultative intracellular pathogen that can cause food poisoning, meningitis, and spontaneous abortions (1). Upon entering a host cell, bacteria begin to express the surface protein ActA (2,3), leading to the nucleation of an F-actin cloud that eventually becomes a polymerizing self-renewing comet tail that propels the bacteria through the host cell cytoplasm and enables them to spread from cell to cell (4). ActA spans the *L. monocytogenes* cell membrane and the thick, highly cross-linked peptidoglycan cell wall (5). Immunofluorescence of the ActA protein shows a polarized distribution on the surface of *L. monocytogenes* (5), which is required for unidirectional bacterial actin-based motility (6). The ActA surface distribution changes throughout the bacterial cell division cycle: dividing bacteria have less protein at the septation zone and more at each pole such that shortly after division most of the protein is localized to the old pole and excluded from the new pole (5). The N-terminus of ActA is exposed to the host cell cytoplasm and interacts with several host cellular proteins including actin and the Arp2/3 complex, nucleating actin filaments at the bacterial surface (7,8). The direct interactions between ActA and proteins of the Ena/VASP (vasodilator-stimulated phosphoprotein) family contribute to cloud formation and subsequent motility characteristics such as speed and path curvature mediated by Ena/VASP's interactions with profilin and with F-actin, respectively (9–11). Most research on *L. monocytogenes* actin-based motility has focused on biochemical and cell biological analysis of steady-state movement, identifying the molecules involved in maintaining and renewing the robust comet tail structure (reviewed in Cameron et al.(12) and Pollard and Borisy (13)). Although several molecular contributors to initial comet tail formation have been identified (9,11,14), comparatively little is understood about the mechanisms by which *L. monocytogenes* initiates movement before reaching a steady state.

The ability to reproduce polymerization-driven motility by using artificial particles in vitro has led to studies of motility initiation in systems with simplified spherical geometry (15–18). However, the motility initiation process of *L. monocytogenes* itself has not been closely examined. The mechanisms by which spherical beads initiate motility in vitro have been described by two classes of biophysical models that depend on bead size and biochemical environment: stochastic symmetry breaking (16) and actin gel strain accumulation (18). In an in vitro system composed of purified proteins, an actin gel is nucleated on the surface of large (up to 10 μm) polystyrene beads coated uniformly with Arp2/3 activator proteins (18). As the gel grows, strain increases and the gel breaks at a random point on the surface to relieve that strain, leading to an asymmetric localization of actin growth and then directly to steady-state movement. In the biochemically more complex environment of cytoplasmic extracts, where actin filament turnover is rapid and gel strain cannot accumulate, only small beads (<1 μm) can initiate motility (15,19). These beads move randomly within their symmetric actin cloud due to stochastic amplification of small fluctuations in the local rate of actin polymerization, thus leading to symmetry breaking and the initiation of unidirectional motility (16).

Although these models are useful to understanding the details of bead motility, they are not general to how *L. monocytogenes* begin to move. Simplified spherical systems have

Submitted February 11, 2005, and accepted for publication June 16, 2005.
Address reprint requests to J. Theriot, Tel.: 650-725-7968; Fax: 650-723-6783; E-mail: theriot@stanford.edu.

0006-3495/05/09/2146/13 $2.00
doi: 10.1529/biophysj.105.061168

a uniform protein distribution. *L. monocytogenes*, however, are intrinsically asymmetric due to their polarized ActA surface distribution and have a more complex rod-shaped geometry. Within the host cell, both beads and bacteria form symmetric actin clouds, yet beads are unable to initiate motility (19), whereas *L. monocytogenes* can do so readily. A necessary next step in understanding motility initiation is to build upon the knowledge obtained from the previously well-characterized simplified systems and incorporate some of the complexity inherent to *L. monocytogenes* itself.

Genetically identical populations of *L. monocytogenes* display great variability in their movement rates within the biochemically uniform environment of cellular extracts (20). At any given time both stationary bacteria associated with symmetric actin clouds and rapidly moving bacteria can be seen. Thus there are variables intrinsic to individual bacteria that have an effect on their motility. One likely possibility is the highly variable polarized ActA distribution on the surface of individual bacteria.

Here we examine the motility initiation process of *L. monocytogenes* in cytoplasmic extracts. The process was found to be highly variable among individual bacteria. Overall, it was comprised of several distinct steps and was characterized by sensitivity to initial conditions and immediate environment during early movement. This sensitivity decreased as motility matured and bacteria reached a robust steady state. We further correlated the different surface distributions of labeled ActA on live bacteria to actin dynamics and movement during initiation and at steady state in a time-resolved manner. Within infected host cells, *L. monocytogenes*' motility initiation was found to depend on the specific cellular environment represented by two different cell types. Despite the great variability in ActA distribution and cytoplasmic environments, all types of bacterial motility initiation eventually converged on the same final result of robust unidirectional polymerization-driven motility.

MATERIALS AND METHODS

Construction of ActA-RFP

PCR amplification and subcloning were performed using standard molecular biology techniques. The plasmid containing the mRFP1 sequence was provided by Roger Tsien (University of California, San Diego). Plasmids pDP-3934, pDP-4035, and pPL1 and *L. monocytogenes* strains DPL-4029, -4083, -4077, and -4087 were provided by Dan Portnoy (University of California, Berkeley). The *Bam*HI-*Kpn*I fragment of pDP-3934 (14) and the C-terminus of ActA (from *Kpn*I) without the stop codon were cloned into pSL1190 (GenBank accession No. U13866). A flexible linker sequence (FNNNVGKVSGFSFPPQLSGLSLS; T. den Blaauwen, University of Amsterdam, personal communication, 2002) was inserted in between ActA and mRFP1 (21). The downstream noncoding region of *L. monocytogenes* genomic DNA following ActA in pDP-3934 through the former SacII site (14) was fused C-terminal to the ActA-RFP (red fluorescent protein) coding sequence in pSL1190 for integration purposes, creating pJT1. The *Bam*HI-*Spe*I fragment of pJT1 was inserted into pPL1, a site-specific phage integration vector for *L. monocytogenes* (22) and integrated by conjugation into DPL-4029 (Δ*ActA* in 10403S background) and DPL-4083 (Δ*ActA* in SLCC-5764 background) as described (22), creating strains JAT-395 and JAT-396, respectively. JAT-395 was used for all infection experiments and JAT-396 for all experiments in extracts. The SLCC-5764 strain contains a constitutively activated mutant of PrfA, the major virulence gene transcription factor in *L. monocytogenes* (23), leading to constitutive expression of ActA in this background. ActA expression levels in JAT-395 and JAT-396 were comparable to DPL4077 and DPL-4087 (22) by Western blot. Motility rates and motility initiation behavior were indistinguishable between DPL-4087 and JAT-396, as was infection and motility of DPL-4077 and JAT-395 in MDCK-GFP-actin (24) and in PtK2-GFP-actin cells.

Strain JAT-433 (ActA mutant GRR-RFP) was created by cloning the *Bam*HI-*Kpn*I fragment of pDP4035 (ActA mutant GRR in pDP-3934 (11,25)) into *Bam*HI-*Kpn*I digested pJT1, creating pJT3, then subcloning into pPL1 and integrating into DPL-4083 (22) as described above.

Motility assays and microscopy

L. monocytogenes in vitro motility assays were performed essentially as described (26). JAT-396 or DPL-4087 *L. monocytogenes* were grown 14–19 h shaking at 37°C in 5 mL Luria-Bertani broth containing 7.5 μg/mL chloramphenicol. A total of 150 μL of 8 mg/mL actin was dialyzed into 5 mM $NaHCO_3$ pH8, 0.2 mM $CaCl_2$, 0.1 mM ATP, 0.1 mM dithiothreitol, then polymerized by addition of KCl and $MgCl_2$ as in Pardee and Spudich (27). This was added to one vial of amine-reactive Alexa-Fluor 488 carboxylic acid tetrafluorophenyl (TFP) ester (Molecular Probes (Eugene, OR) A10235) and quenched after 2 h with 7 μL buffered hydroxamine. The labeled actin was cycled through two rounds of polymerization and depolymerization (27). A total of 25 μL *Xenopus laevis* egg extract, 2.5 μL ATP regenerating mix (28), and 2 μl of Alexa-488 labeled actin (1.1 mg/mL, 0.5 dyes/actin) were mixed and diluted with *Xenopus* buffer (28) such that the final motility assay would be 40%, 50%, or 60% of the original extract concentration, then kept on ice; 1 μL resuspended bacteria and 1 μL 0.9 or 1.8 μm prediluted silica spacer beads were added to 5 μl extract mixture. A total of 1.2 μL of the mixture was immediately spread between a glass slide and 22 mm square coverslip, sealed with VALAP (vaseline/lanolin/paraffin, 1:1:1), and used for microscopy of motility initiation. As a control experiment, both the slide and coverslip were precoated with 4 mg/mL bovine serum albumin, which did not alter the steps or progression of motility initiation. Microscopy was performed using a Zeiss (Thornwood, NY) Axioplan microscope equipped with phase contrast and epifluorescence optics. Time-lapse images were collected on a cooled charge-coupled device camera (MicroMax 512BFT; Princeton Instruments; Trenton, NJ) every 5 s in each fluorescence channel using MetaMorph software (Universal Imaging; Downington, PA). Deblurring of images in Fig. 1 was performed using AutoDeblur 9.2 software (AutoQuant Imaging, Watervliet, NY).

Bacterial tracking

Analysis was performed using automated tracking software customized for *L. monocytogenes* moving in *Xenopus* extract (20). Phase-dense objects were identified using a threshold algorithm optimized for each time-lapse movie. Limits for object size, maximum displacement between frames, and minimum track length (10 frames) were specified. Each tracked object was stored as a set of intensity values in the phase, actin, and ActA channels for a 64 × 64 pixel box surrounding the object's centroid, aligned with the object's long and wide axes for each frame. Additional parameters were determined including the coordinates of the object centroid, the average length and width, and the timing of each frame in a movie. Only in-focus bacteria were included in the data set, and all actin-associated bacteria were classified into motility initiation subgroups including those that nucleated actin clouds de novo, started moving, hopped, and stopped hopping. For tracked bacteria with interrupted trajectories, only the first set of positions was included in the analyzed data set. All examples used to describe stages

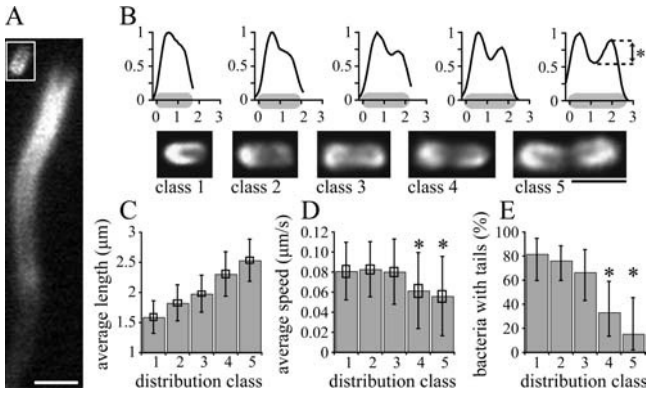

FIGURE 1 ActA distribution class affects speed and tail formation. (*A*) A bacterium expressing ActA-RFP associated with an actin comet tail in cytoplasmic extract. Inset shows ActA distribution. The actin tail formed at the end with more ActA (*rear*). Bar is 2 μm. (*B*) Representative individual examples of the five ActA-RFP surface distribution classes found for *L. monocytogenes* quantitated by calculating the average relative intensity at each point along the bacterial length (position in micrometers from rear). Shaded bacterial outlines represent the length of each example bacterium shown in each class. Asterisk on the far right indicates the metric used to categorize classes 3–5. Bar is 2 μm. (*C*) Average bacterial length in classes 1–5, calculated for 23, 38, 54, 34, and 45 bacteria, respectively. ActA distributions correlated with bacterial length. Each point is significantly different from all others ($p < 0.05$ by rank sum test (46)). (*D*) Average steady-state speed of bacteria for each distribution class. Bacteria of distribution classes 1, 2, and 3 moved at significantly greater speeds than classes 4 and 5 (see *asterisks*, $p < 0.05$ by rank sum test. Error bars show standard deviations, and boxes show standard error). (*E*) Percentage of a subpopulation of bacteria associated with actin tails at 10 min after mixing (112 total bacteria). Bacteria of distribution classes 1, 2, and 3 had a significantly greater percentage of tails than classes 4 and 5 (*asterisks*; *z*-test, $p < 0.05$). Error bars show 95% confidence interval.

of motility initiation were representative of a final filtered data set used for quantitative analysis including 279 actin-associated bacteria in 26 movies taken over 6 days with two separate batches of extract. Additional movies used in preliminary analysis of motility initiation contributed to a total of >500 bacteria imaged during motility initiation. An additional 201 bacteria were analyzed at steady state for comparison. Movies of ActA and actin linescan traces over time were created using a script in Kaleidograph 3.6 (Synergy, Reading, PA) and QuicktimePro.

Classification of ActA distributions

During imaging of motility in cytoplasmic extracts, *L. monocytogenes* remained alive but did not continue to grow, which effectively provided a static ActA distribution specific to each bacterium and also spanned the full range of ActA distributions throughout the bacterial division cycle within the overall population. Due to ActA-RFP photobleaching, analysis of the surface distribution was performed on the first frame of the movie. For each bacterium, the width at its center was determined using the phase channel, and at each position along its length (and extending two pixels beyond each end) an average intensity in the ActA-RFP fluorescence channel spanning that width was calculated, creating the linescan intensity profile. Normalization included first subtracting the minimum value two pixels beyond the edge in the first three frames and then scaling intensities from zero to one. For example images of ActA distributions, the first frame in a movie was used for maximum signal.

Actin distributions and bacterial speed

Actin linescan intensity profiles were quantitated in the same way as for ActA and extended two or more pixels beyond each end of the bacterium, depending on the example. Normalization was performed over all frames of a tracked bacterium. The speed was determined as the displacement over time in micrometers per second (by calibration) of the centroid position from one frame to the next. Actin intensities and speed were plotted such that each point on the *x* axis represents one frame of the movie and then colorized with the graphing software package in IgorPro 4.05 Carbon.

ActA and actin distributions around the bacterial circumference

The fluorescence intensity was determined at any point on the bacterial circumference established by a given angle between the rear of the bacterium and the point of interest. Angles to the right of the direction of movement were positive and to the left were negative, from 0° to 180°. The intensities at the edge and one pixel inward and outward along the radial line between the centroid and the edge were averaged. De novo actin accumulation was quantitated at specific angles. Intensities at points along the sides were averaged over both sides and normalized as above.

Classification of moving bacteria

To determine the percentage of bacteria in each distribution class moving at 10 min after addition to extract, a subset of the full data set was used in which bacteria were imaged under comparable conditions (same extract batch) and in the correct time range (112 bacteria). For most bacteria, classification for moving with a tail was visually uncomplicated. For questionable cases, the position of peak actin intensity needed to be over 0.02 μm beyond the edge of the bacterium to be classified as a tail. Bacteria moving at steady state were determined in the same way.

L. monocytogenes infections and analysis within cells

Potoroo tridactylis kidney epithelial (PtK2) cells were transfected with pEGFP-actin kindly provided by Angela Barth and James Nelson (24) using FuGENE6 (Roche, Pleasanton, CA), selected for stable transfectants with 400 μg/mL G418 (geneticin; Gibco/Invitrogen; Carlsbad, CA), and FACS (fluorescent-activated cell sorter) sorted twice for GFP (green fluorescent protein) fluorescence (with the Stanford Shared FACS Facility). JAT-395 and 10403S *L. monocytogenes* were used to infect GFP-actin-expressing PtK2 and Madin Darby canine kidney (MDCK) cells essentially as described previously (24,29). Cells were maintained in DME (Dulbecco's modified Eagle's) medium supplemented with 10% fetal bovine serum (FBS) (Gemini Bio-Products; Woodland, CA) and 1% antibiotic-antimycotic (ABAM) (Gibco/Invitrogen). Cells were plated onto 25 mm round coverslips in 6-well tissue culture dishes in 2 mL DME + FBS medium 24 h before infection such that cell confluency would be 40–60% at infection. 10403S and JAT-395 *L. monocytogenes* were grown 14–18 h in liquid brain heart infusion (BHI) medium (7.5 μg/mL chloramphenicol for JAT-395) without agitation at room temperature. Bacteria were spun down in a microcentrifuge for 1–2 min and resuspended in half the original volume PBS, then 150–300 μL were used to infect each coverslip. Bacteria were added to the cells for 1 h, then the cells were washed twice in 3 mL DME + FBS medium and left another 30 min at which point gentamycin was added to each coverslip (20 μg/mL).

Time-lapse images were collected using a 60× 1.4 N.A. objective on a Nikon Diaphot-300 inverted microscope equipped with a cooled charge-coupled device camera (MicroMax 512BFT; Princeton Instruments). Phase-contrast and epifluorescence video microscopy was performed by imaging

cells on a coverslip bathed in Leibovitz's L15 medium (Gibco/Invitrogen) at 37°C using a temperature-controlled chamber connected to a circulating water bath. Time-lapse images were collected every 5 or 10 s in each necessary channel using MetaMorph software (Universal Imaging).

Motility initiation events were quantitated in 13 MDCK (all expressing actin-GFP) and 12 PtK2 cells (eight expressing actin-GFP) infected with either wild-type 10403S or JAT-395 *L. monocytogenes* between 2 and 6 h after infection. Motility initiation events were counted within each 10 min interval in the time-lapse movies of these infected cells. A bacterium initiating movement with division was scored as a single event. Division-initiation events were scored as occurring concurrently if both bacteria formed tails and began moving within <2 min of each other. In 3 of 69 initiation events, the second bacterium began moving more than 10 min later than the first and was therefore counted as a separate initiation event within the next 10 min interval.

RESULTS

Bacterial speed and tail formation correlated to ActA surface distribution

We fused monomeric red fluorescent protein (mRFP1) (21) to the C-terminus (cytoplasmic tail) of the ActA protein, separated by a flexible linker sequence to minimize steric hindrance between molecules in the context of a very high ActA density on the bacterial surface. The expression of this fusion protein in a Δ*actA* background was regulated by the endogenous *actA* promoter in single copy within the genome and was equivalent to wild-type ActA integrated in the same manner (see Materials and Methods). *L. monocytogenes* expressing ActA-RFP were able to infect cells normally, and their actin-based motility was indistinguishable from bacteria expressing wild-type ActA, both in infected cells (strain JAT-395 derived from strain 10403S, which expresses ActA only after invading a host cell (2,3)) and in cytoplasmic extract (strain JAT-396 derived from strain SLCC-5764, which constitutively expresses ActA and other virulence factors (23)). As expected (4,30), over 90% of actin comet tails associated with the pole of *L. monocytogenes* with a higher density of the ActA-RFP protein (*rear*; Fig. 1 *A*).

We performed time-lapse video microscopy of initiation and steady-state movement on bacteria moving in cytoplasmic extract. A continuum of ActA surface distributions within the population correlated with bacterial length and therefore bacterial division cycle (Fig. 1) and for convenience in further analysis was divided into five classes. The shortest bacteria, those that had recently divided, showed a single peak of ActA fluorescence at one pole, with a decreasing gradient along their length (class 1, average length 1.6 μm, Fig. 1, *B* and *C*). For slightly longer bacteria, ActA had started accumulating at the opposite new pole (former septation zone) and had concurrently been excluded from the nascent septation zone such that the linescan displayed a shoulder in the polar distribution profile (class 2, 1.8 μm, Fig. 1, *B* and *C*). In successively longer bacteria, the shoulder increased in intensity and became a second distinct peak (classes 3, 4, and 5; 2.0 μm, 2.3 μm, and 2.6 μm, Fig. 1, *B* and *C*). Classes 3, 4, and 5 were distinguished by calculating the relative difference in fluorescence intensity between the septation zone and the second peak as a percentage of the primary peak intensity, and bacteria were grouped into classes of 0–10% (class 3), 10–20% (class 4), and $>20\%$ (class 5; *asterisk* in Fig. 1 *B*). In a population of 201 bacteria, only 7 could not be placed in any class, and all other bacteria were distributed rather evenly among the five distribution classes.

To see whether ActA distribution profiles had any influence on actin-based motility, we correlated ActA distribution class with average speed per bacterium for 194 bacteria associated with actin tails and moving at steady-state speed (45 min to 2 h after addition to extract). Bacteria with ActA distributions classes 1, 2, and 3 moved at indistinguishable average speeds of 0.081, 0.083, and 0.078 μm/s, whereas those with distribution classes 4 and 5 moved at 0.063 and 0.056 μm/s, respectively, significantly slower than the other distribution classes ($p < 0.05$; Fig. 1 *D*). Thus more bipolar ActA surface distributions correlated with slower steady-state bacterial speeds.

The overall motility initiation process can be seen for a population of bacteria in Movie 1 in the Supplementary Materials. This movie highlights the diversity in motile behavior among individual bacteria during initiation and demonstrates the overall maturation process as bacteria accumulated actin clouds, began to move, and eventually were associated with robust actin comet tails by the end of the movie. Systematic differences in timing of tail formation were correlated to ActA distribution classes. Classes 4 and 5 showed a significant difference in the percentage of bacteria associated with an actin tail at 10 min after mixing with extract, compared with the other classes (Fig. 1 *E*; $p < 0.05$ for all pairwise comparisons). A monotonic decrease in the frequency of tail association was apparent for successively more bipolar bacteria. These results prompted us to consider bacteria with little or no ActA at the second pole (unipolar classes 1, 2, and 3) separately from those with a distinct second peak of ActA intensity (bipolar classes 4 and 5) during the initiation process. We then systematically classified distinct steps in the overall initiation process and examined motility at each step quantitatively.

Initial actin-based motility linked to cloud formation dynamics

Immediately after *L. monocytogenes* constitutively expressing ActA-RFP were added to cytoplasmic extract, they were not associated with any actin and moved by Brownian motion. Within 5 min, actin began to accumulate on the bacterial surface, and the bacteria became immobilized. We quantitated the distributions of actin and ActA on the surface of bacteria during cloud formation and motility initiation for 118 bacteria. Representative examples of unipolar and bipolar bacteria initiating movement are shown in Fig. 2, *A*

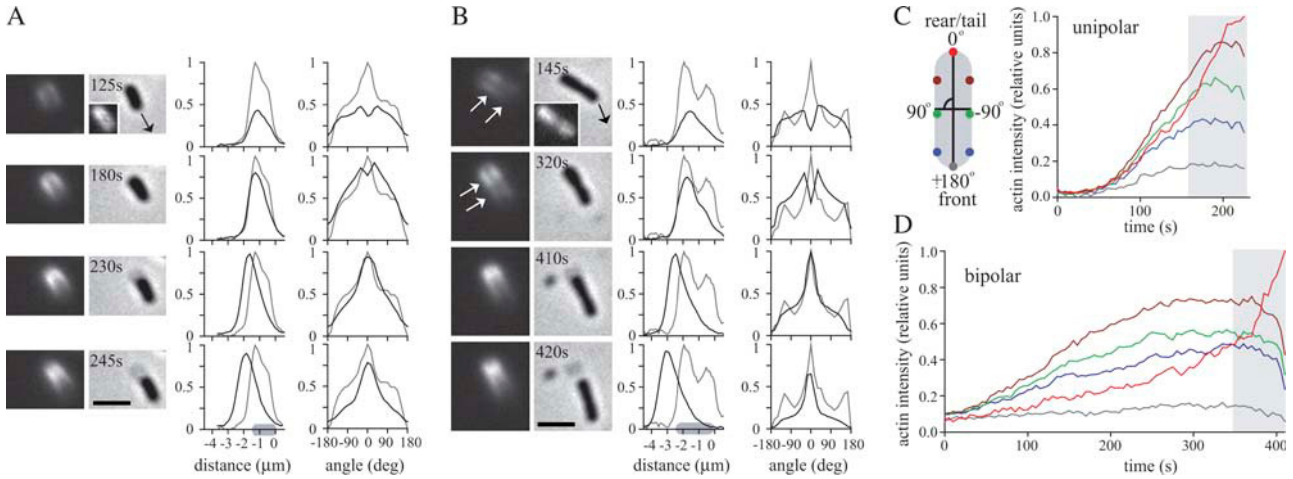

FIGURE 2 Initial cloud accumulation and movement of *L. monocytogenes*. A time course of actin accumulation, polar cloud formation, and initial movement for a representative bacterium with a unipolar (*A*, class 2) and a bipolar (*B*, class 5) ActA distribution. (*A* and *B*) Left panels show actin fluorescence and right panels show phase contrast. Insets shown in the earliest panel are ActA distributions in the first frame of the movie. Arrows in the phase-contrast images indicate the future direction of movement. Right graph panels are relative fluorescence intensities along the length of the bacterium (0 is the front), indicated in gray on the *x* axis in the latest panel (position in micrometers; *left graph*; linescan intensity), and around the circumference of the bacterium (0° is the rear of the bacterium, seen in *C*; *right graph*; radial intensity). ActA distribution, gray line, is calculated from the first frame of the movie, whereas the actin distribution, black line, changes for each image. (*A*) Initial actin accumulation correlated with the unipolar ActA distribution profile (125 s), with accumulation along the sides near the rear end and less directly at the pole. As lateral actin accumulation continued, the bacterium slowly moved forward (180 s). Actin then began to accumulate directly at the rear pole and less along the sides as the cloud became fully polar and reached its maximum intensity (230 s). The polar actin cloud rapidly turned into an actin tail, with weaker intensity along the bacterial surface and a fast burst of speed (245 s). Bar is 2 μm. (*B*) Initial actin cloud formation correlated with the bipolar ActA distribution profile (145–320 s). Actin was visible near both ends (*white arrows*) and less at the septation zone. More ActA was visible along the sides of the bacterium than at either pole. Notice the shoulder in the actin distribution in the linescan intensity graph and the small peaks near the front of the bacterium ($\pm$180°) on the radial intensities graph at 320 s. As actin continued to accumulate along the sides, the bacterium slowly moved forward. Actin then began to accumulate directly at the rear pole of the bacterium, forming a polar actin cloud (410 s) characterized by a continuous distribution gradient of actin on the surface from the front to the rear spanning the septation zone, less actin along the sides, and a more rearward position of the actin peak. The formation of a polar actin cloud took longer than for the unipolar example. Bar is 2 μm. (*C* and *D*) Relative actin intensities over time at specific positions on the bacterial surface before tail formation. Intensities at the points on both sides of the bacterium were averaged. Curves are color coded with position around bacterial circumference (and include the rear and front as well as 45°, 90°, and 135° in each direction). The shaded region indicates the period of forward movement.

and *B*. On bacteria with unipolar ActA distributions, initial actin accumulation correlated with the ActA distribution profile along the bacterial length (Fig. 2 *A*, linescan intensity graphs at 125 and 180 s); more actin accumulated near the rear. Quantitation of the protein distribution around the circumference of the bacteria showed that actin initially accumulated along the sides near the rear end (Fig. 2 *A*; radial intensity graphs at 125 and 180 s). As actin continued to accumulate laterally, bacteria began to move forward slowly (Fig. 2 *A*, 180–230 s). Actin then accumulated directly at the rear pole, and a polar cloud was formed by 230 s. Polar cloud formation was characterized by the rearward movement of the position of peak actin intensity along the long axis (see linescan) in the bacterial frame of reference as well as by an increase in actin accumulation at the rear pole of the bacteria and a decrease along the sides (Fig. 2 *A*, 230 s). At various times after polar cloud formation, bacteria moved with a burst of speed, and the intensity of actin on the bacterial surface decreased as they left the bright actin cloud behind and formed a tail (Fig. 2 *A*, between 230 and 245 s). Quantitation of actin accumulation at specific points on the bacterial surface showed early accumulation along the sides of the bacterium and later more rapid accumulation directly at the rear pole (0°) as the intensity at the sides decreased (Fig. 2 *C*) and the bacterium began to move forward (*shaded region* in Fig. 2 *C*). Among 78 bacteria imaged during cloud formation, 95% showed a greater accumulation of actin along the sides than at the rear before movement.

The initial accumulation of actin along the sides of bacteria when the greatest concentration of ActA occurred at the poles was surprising. It has been previously reported that an actin gel becomes thicker when the geometry of the surface it is growing on is less curved, presumably because gel strain accumulates more slowly on flatter surfaces (17). We found that beads of a size comparable to the hemispherical poles of *L. monocytogenes* (0.5 μm diameter) coated with equivalent concentrations of ActA accumulated actin clouds much more slowly (first clouds appearing 20 min after mixing) than larger beads comparable in size to the cylindrical bacterial sides (2 μm diameter; all beads associated with clouds within 2 min after mixing; data not shown). Therefore, it appears that bacterial surface shape as well as ActA density influence the initial rate of actin accumulation at different points on the surface.

For bacteria with a bipolar ActA distribution (classes 4 and 5), initial actin accumulation was bipolar and correlated with the ActA distribution along the length of the bacterium, with most of the actin accumulating along the sides near the rear end. Some lateral accumulation was also visible near the front, whereas the septation zone accumulated the least, effectively dividing the bacterium into two regions of actin accumulation (*graphs* and *arrows* in Fig. 2 *B* shown at 145 and 320 s). The bacterium eventually began to move forward slowly, and the actin distribution profile evolved until a polar actin cloud resembling that of unipolar bacteria was formed by 410 s. The polar cloud was characterized by more actin at the rear and less along the sides and a continuous actin gradient along the full length of the bacterium, with little or no actin near the front end. Once a polar cloud formed, the transition to an actin tail was similar to that for unipolar ActA bacteria (compare Fig. 2 *A* at 245 s with Fig. 2 *B* at 420 s). Actin accumulation at specific points on the bacterial surface (Fig. 2 *D*) showed early and gradual accumulation along the sides and later, more rapid, accumulation at the rear. Actin accumulation dynamics and polar cloud formation were slower for bipolar ActA bacteria (compare Fig. 2, *C* and *D*), and differences in tail formation seen in Fig. 1 *E* could be due to a delay caused by competition for actin accumulation and cloud formation at each end in bipolar bacteria. Thus the initial movement of *L. monocytogenes* and its initial tail formation depended in a complex manner on the polar nature of ActA distribution and the rod-shaped bacterial geometry (see Movies 2 and 3).

Competition for actin accumulation between both ends of bacteria with bipolar ActA distributions

The example bipolar ActA bacterium shown in Fig. 2 *B* initially accumulated actin laterally at both ends. The rear end with more actin, however, consistently dominated during the entire process of polar cloud formation, and the front lost its association with actin. A different situation was seen for another, more bipolar (class 5) bacterium in the process of initiating motility (Fig. 3 *A*). Initially, actin accumulated along the sides at both ends as in Fig. 2 *B* but then the front, instead of the rear, end began to form a polar cloud and caused the bacterium to move slowly backward (Fig. 3 *A*, 300–500 s). This polar cloud, however, was unable to turn into an actin tail. The intensity of the cloud decreased, and the actin distribution profile reverted to lateral accumulation near both ends of the bacterium (Fig. 3 *A*, 700 s). The rear then became dominant and formed a polar cloud, which was able to successfully turn into an actin tail as the bacterium initiated motility (Fig. 3 *A*; 800–850 s and Movie 4). This ability in bipolar bacteria for the front end to accumulate actin was also seen occasionally on some bacteria after they had already started moving (Fig. 3 *B*, see the distinct actin peak in the linescan *insets* in I and III). Perhaps bipolar bacteria with two distinct peaks of ActA experienced competition for actin accumulation between both ends, which led to a delay in polar cloud formation at the rear as actin exerted forces at both ends of the bacterium. This would explain both the delay in tail formation (Fig. 1 *E*) and slower steady-state movement (Fig. 1 *D*) that we observed for bipolar bacteria.

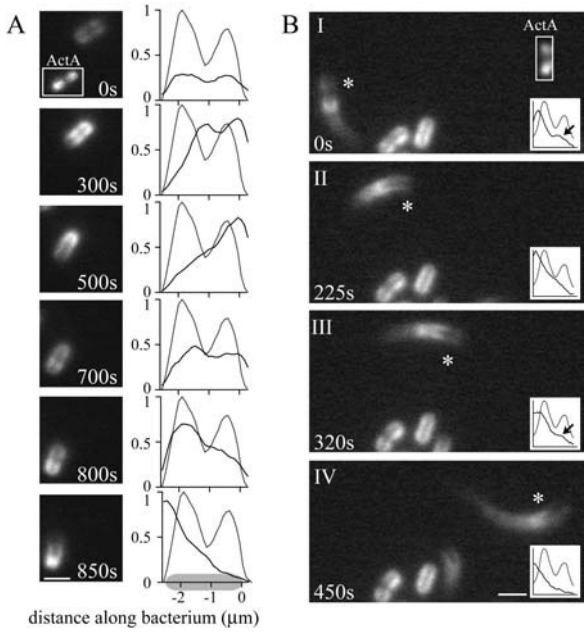

FIGURE 3 Both ends of a bipolar ActA bacterium (class 5) compete for actin accumulation and cloud formation. (*A*) Time course of cloud and tail formation for a bipolar ActA bacterium. Left panels show actin fluorescence, and inset is ActA fluorescence in the first frame of the movie. Right panels show ActA (*gray*) and actin (*black*) linescans along the length of the bacterium (indicated in *shaded area* along the *x* axis). The first image was taken ~12 min after mixing bacteria with extract. Bar is 2 μm. (*B*) A bipolar ActA bacterium (class 5) associated with an actin tail. Image shows actin fluorescence, top right inset is ActA, and bottom right inset is the linescan of ActA (*gray*) and actin (*black*) for each panel. Panels I and III show that the front end sometimes nucleated an actin cloud, seen as a distinct peak in the linescan (*arrows*), but this did not occur at all times during movement. Panels II and IV show the polar actin distribution along the bacterium typical of normal tails. Bar is 2 μm.

Speed bursts and sudden stops characteristic of early motility

Next we examined the early movement of *L. monocytogenes* once they had formed an actin tail and began moving. Instead of continuing at steady state immediately after movement initiation, bacteria underwent rapid, erratic bursts of speeds and sudden, often complete, stops during which they moved very slowly or not at all. These erratic changes in speed resulted in actin tails of a discontinuous nature during this hopping regime of initiation (Fig. 4 *A*). Out of over 500 bacteria imaged during initiation, not a single one started moving continuously at steady state without stopping. Fig. 4

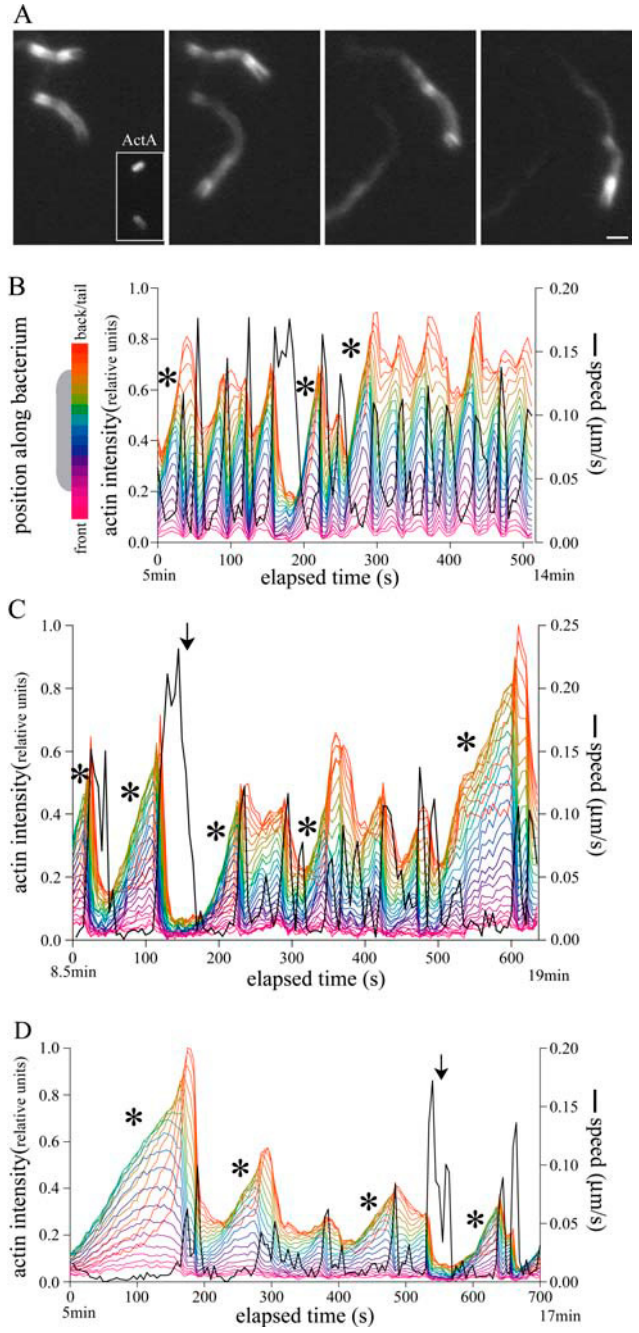

FIGURE 4 Early hopping regime of motility initiation. (*A*) Two bacteria with discontinuous hopping actin tails starting at ~5 min after addition to extract (fluorescent actin). Inset in the earliest panel is the ActA signal on the bacteria. The top bacterium is graphed in *B*. Bar is 2 μm. (*B*) Graph of top bacterium in *A*, displaying the instantaneous speed trace (in *black* along the *right* axis) and a color coded trace of relative fluorescence intensity over time, with each color representing a position along the bacterial surface. Asterisks indicate polar cloud formation before bursts of speed. Lower labels on the *x* axis refer to the approximate time since mixing of the bacterium and extract. Movie 6 in the Supplementary Materials shows the frame-by-frame image sequence of the bacterium and its actin intensity distribution for each frame to reference with this graph. (*C* and *D*) Two further examples of ''hopping'' bacteria (Movies 7 and 8). Note the different speeds for *C*. Arrow indicates a time in the trajectory when the bacterium lost association with its actin tail, tumbled randomly, slowed after interactions with other components in the extract, and reinitiated motility (see phase image in Movie 7).

A shows two representative *L. monocytogenes* at ~5 min after they were added to the extract after the cloud and tail have already formed. Both bacteria demonstrated a typical discontinuous tail characteristic of hopping (Movie 6). The graph in Fig. 4 *B* displays the speed trace (in *black*) through time for one of the two bacteria (*asterisk*). The normalized actin linescan intensity is plotted for each pixel position along the bacterial long axis for each time point. Two additional examples of hopping bacterial motility can be seen in Fig. 4, *C* and *D* (corresponding Movies 7 and 8). These three graphs are representative of the variability in motility during the hopping regime and demonstrate the trends found in the 224 bacteria analyzed during this early regime of motility.

The bursts of speed were preceded by accumulation of a polar actin cloud (*asterisks* in Fig. 4, B–D) and were significantly faster than the speeds characteristic of steady state at or above 0.2 μm/s (compare with Fig. 1 *D*). Polar cloud formation was characterized by a rearward movement of the position of peak actin intensity in the bacterial frame of reference, seen as a sequential color change on the intensity graphs (*asterisks*). The intensity of the actin tail was very weak during the bursts and correlated somewhat with speed (Fig. 4 *B*, faster speed bursts had weaker tails). After a very rapid burst of speed, all association with the tail could be lost; the bacterium would tumble randomly until it interacted with a physical obstruction, such as a vesicle in the extract or another tail, stopped, and then reaccumulated actin and reinitiated motility as described in the previous section (*arrows* in Fig. 4, *C* and *D*). No regular periodicity in speed variation as a function of time or distance traveled could be found even within a single bacterium's trace. The bursts of speed were not correlated to the rate of actin cloud formation nor to the maximum intensity of the cloud. The most noticeable trend during the hopping regime of motility initiation was the considerable degree of variation among individual bacteria.

Transition to steady state and robust motility

Over time, bacterial motility matured and reached steady state, such that erratic hopping was generally not observed beyond 30 min after mixing. Bacteria stopped less frequently and moved continuously for longer durations and distances. The morphology of the actin tail changed from discontinuous (Fig. 5 *A*) to long and weak (Fig. 5 *B*) and eventually to a bright, short form characteristic of stable robust actin comet tails (Fig. 5 *C*) (20). In general, most bacteria began to be associated with continuous longer, weaker tails 20–30 min after mixing with extract, and actin tails were bright and stable by 45 min (Movie 1). The leftmost example in Fig. 5, *A–C*, shows a single bacterium over time, and its speed and

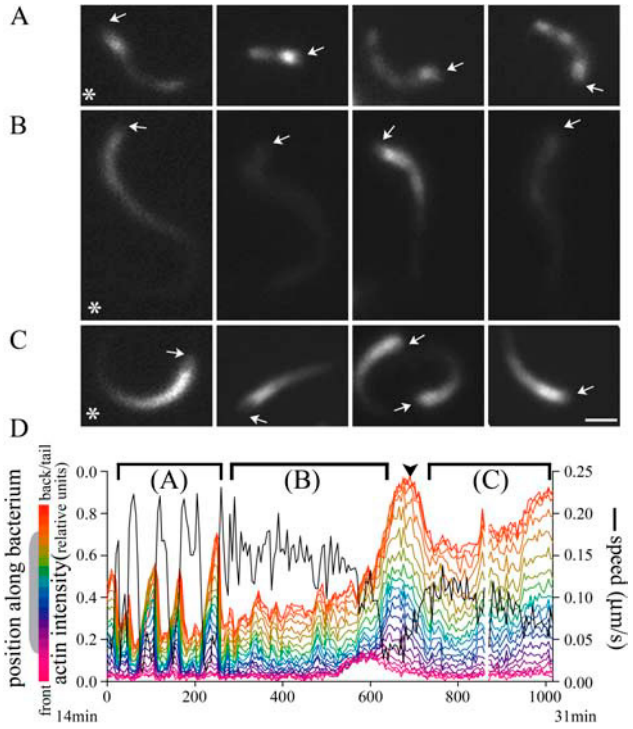

FIGURE 5 Maturation of the actin tail and transition into steady-state motility. (*A*) Images of hopping tails early in initiation as in Fig. 4. (*B*) Actin tails 20–30 min after mixing. Tails were no longer discontinuous; rather, they were very long and weak in intensity. (*C*) Bright, shorter, steady-state actin tails imaged 30 min and later after mixing with extract. Arrows indicate positions of bacteria. Bar is 2 μm. (*D*) Graph of bacterial speed and actin intensities for each frame of the individual bacterium marked with an asterisk in *A–C*. Brackets refer to the three phases of maturation seen in the images. Arrowhead indicates loss of speed when the bacterium ran into its own tail but rapidly recovered steady-state motility. Lower labels on *x* axis refer to approximate time since mixing bacteria and extract.

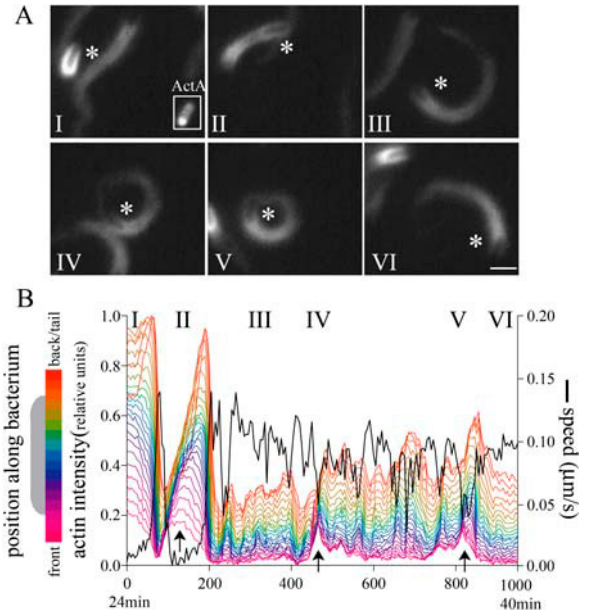

FIGURE 6 Decrease in sensitivity to the environment associated with the transition into steady state. (*A*) A bacterium, indicated by the asterisk, initiated motility (*I*) then stopped suddenly and dramatically due to another tail in its path (*II*), which caused it to reinitiate motility and hop again. Its trajectory was interrupted twice more by another and its own tail (*IV* and *V*) without much effect on its tail intensity or speed. The inset shows the ActA distribution. Bar is 2 μm. (*B*) Speed and actin intensity graph of the bacterium in *A*. Roman numerals on the graph refer to time points in part *A* for comparison. Arrows mark the increase in actin near the front of the bacterium during the collisions. Notice the dramatic stop and reinitiation of a polar cloud at *II* and the comparatively slight reductions in speed at *IV* and *V*. Lower labels on the *x* axis refer to the time since mixing of the bacterium and extract.

actin intensities trace is seen in Fig. 5 *D*. The gradual maturation of the tail through loss of speed bursts and gain of tail intensity can be seen (Movie 9).

Concurrently with changes in actin tail morphology as bacteria stopped hopping and began to move more persistently, motility of these bacteria also became less sensitive to obstructions in the environment. During the hopping regime of motility, bacteria often stopped completely and reinitiated motility after even slight interactions with vesicles in the extract or with small remnants of a depolymerizing actin tail from another bacterium in their path, displaying great sensitivity to their environment. The decreased sensitivity can be seen in Fig. 5 *D*, when the bacterium ran into its own tail (*arrowhead* and see Movie 9) but recovered quickly and continued to mature without any erratic hopping movement. Another example of decrease in sensitivity during maturation is shown in Fig. 6 in which a bacterium encounters its own and other tails in its path three times. In contrast to the earliest interruption, which caused a complete stop (II), the later two affected the bacterium to a much lesser extent as it was further on in the maturation process (IV and V); it only slightly decreased its speed as it continued its persistent motility (Movie 10).

Interaction between ActA and VASP contributes to motility maturation

The direct interaction between the ActA proline-rich region and members of the Ena/VASP proteins has been implicated in discontinuous comet tails and hopping motility (31,32). We created a fusion between the ActA GRR mutant (defective for VASP binding (11,25)) and mRFP1 (JAT-433) and compared the motility initiation process to wild-type ActA-expressing bacteria. We saw no differences in the ActA surface distribution or the levels of RFP signal on the surface of individual bacteria. Mutant bacteria, however, had a delay in cloud formation, similar to previous observations in infected cells (11). Ten minutes after mixing wild-type bacteria with extract, 64% were associated with an actin cloud, 23% were moving with an actin tail (hopping), and 13% were not associated with any actin ($n = 56$ bacteria). In a directly comparable experiment 10 min after mutant bac-

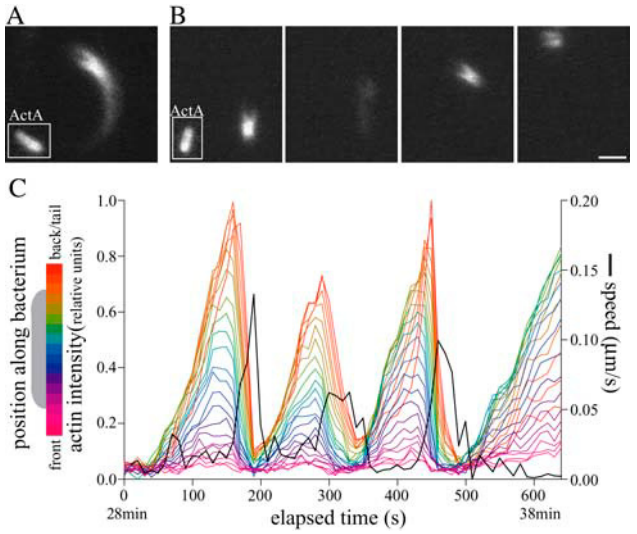

FIGURE 7 Motility initiation of ActA GRR mutant bacteria. (*A*) Bacterium expressing wild-type ActA-RFP associated with a steady-state actin tail at 25 min after mixing with extract. (*B*) Bacterium expressing mutant GRR-RFP associated with a hopping tail between 30 and 35 min after mixing. Depolymerization of the unstable tails is very rapid such that often bacteria seem to be associated with an actin cloud or very short actin tail, distinct from the hopping motility of wild-type bacteria (Fig. 4 *A*). Panels show actin fluorescence, and insets show ActA fluorescence in the first frame of the movie. Bar is 2 μm. (*C*) Speed and actin intensity graph of the bacterium in *B*. Notice the extreme bursts of actin accumulation and speeds and complete stops and loss of actin more severe than for wild-type hopping bacteria (Fig. 4, *B–D*).

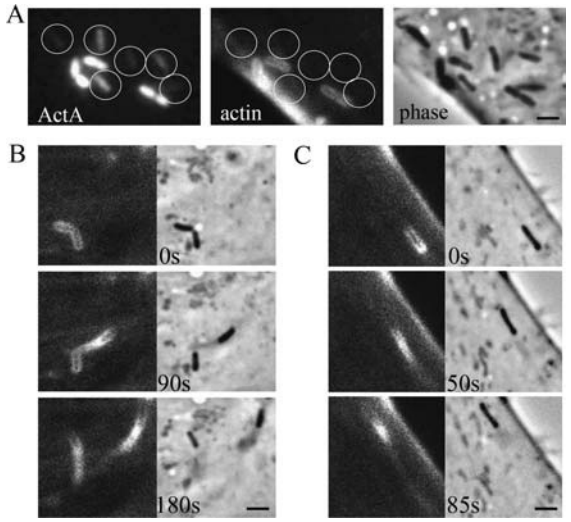

FIGURE 8 Cloud and tail formation on *L. monocytogenes* inside host cells. (*A*) Several ActA-RFP-expressing *L. monocytogenes* inside an MDCK cell expressing actin-GFP. The left panel shows ActA fluorescence, the middle panel shows actin, and the right panel shows phase contrast. Circles indicate bacteria with low levels of ActA that were not associated with an actin cloud. (*B*) *L. monocytogenes* inside a PtK2 cell, expressing actin-GFP that divided and initiated movement with division. Both daughter bacteria began moving concurrently. The left panel shows actin fluorescence, and the right panel shows phase contrast. (*C*) *L. monocytogenes* initiated movement inside a PtK2 cell without division, forming a polar cloud and then a tail as in Fig. 2. Bar is 2 μm.

teria were mixed with extract, 27% were associated with an actin cloud, 16% with an actin tail (hopping), and 57% were not associated with any actin ($n = 37$ bacteria). Wild-type bacteria in this experiment formed robust comet tails at 25 min after mixing with extract (Fig. 7 *A*). However, no mutant bacteria were seen moving without erratic hopping at 40 min after mixing (Fig. 7, *B* and *C*), not even having reached the intermediate stage of maturation in which wild-type bacteria are normally associated with longer, weak comet tails (Fig. 5 *B*). Whereas wild-type bacteria moving in the hopping regime were often visibly associated with discontinuous actin tails (Figs. 4 *A* and 5 *A*), mutant bacteria displayed more extreme bursts of movement and sudden stops with rapid depolymerization of their comet tails such that at any time they could seem to be associated with an actin cloud instead of a tail (Fig. 7 *B* and Movie 11). Actin clouds and tails were often of weaker intensity than seen on wild-type bacteria.

Motility initiation varies in different cell types

Within an infected host cell, *L. monocytogenes* spend up to several hours associated with a symmetric actin cloud before forming tails and initiating movement (4). *actA* is transcribed only after the bacteria enter the host cell, as early as 30–60 min after infection, and actin cloud formation is correlated to *actA* transcription as ActA protein expression levels rise and the infection proceeds (3). We wished to investigate the connection between the amount of ActA on the bacterial surface and actin cloud formation. In a cell infected with multiple bacteria, only those individual bacteria with higher amounts of ActA were associated with actin clouds, whereas those with less ActA on their surface (*circles*) were not (Fig. 8 *A*). Bacteria were often seen associated with actin clouds in which the actin intensity along the bacterial sides was greater than at the rear, especially early after infection (1.5–3 h), similar to initial actin accumulation on bacteria in extracts (data not shown).

The motility initiation process in extracts was shown to be very sensitive to heterogeneities in the environment. An infected host cell has its own dynamic cytoarchitecture which can influence bacterial movement (29), and we wished to examine motility initiation in two epithelial cell types with distinct cellular environments: the columnar MDCK cell and the flattened squamous PtK2 cell. *L. monocytogenes* initiated movement in two different ways within MDCK and PtK2 cells expressing actin-GFP (24). First, some bacteria associated with a symmetric actin cloud were seen to divide, and upon division the two daughter cells were both associated with polar actin clouds that could become actin tails (Fig. 8

B). Second, other bacteria associated with polar actin clouds initiated movement without division as the clouds turned into tails as in cytoplasmic extracts (Fig. 8 *C*, Movies 12 and 13). The number of motility initiation events within 10 min intervals was counted in both cell types. Between 2 and 6 h after infection, 21 of 26 bacteria (81%) initiating movement in MDCK cells did so with division. Fifteen of these 21 division-initiation events (71%) led to both daughter bacteria concurrently forming tails and initiating motility (<2 min between each bacterium initiating movement). In PtK2 cells, 20 of 43 bacteria (47%) initiated motility with division, and only 7 of these 20 division-initiation events (35%) led to concurrent motility initiation of both daughter cells. The kinetics of the motility initiation process was thus dependent on the cellular environment in PtK2 and MDCK cells.

DISCUSSION

Motility initiation affected by bacterial geometry and ActA surface distribution

Here we have shown that motility initiation for *L. monocytogenes* is a complicated, multistep process in contrast to the simple symmetry-breaking process observed for uniformly coated spherical beads. Although ActA-coated beads are able to move in both cytoplasmic extracts (15) and in a reconstituted system of purified proteins (31), they are unable to break the symmetry of their actin clouds when introduced into a living host cell (19). The complexity inherent to *L. monocytogenes*' rod-shape geometry and polar ActA surface distribution greatly affects the initiation of motility. Furthermore, this dependence leads to variation in the dynamics of motility initiation in various environments including extracts and different host cell types.

The initial accumulation of actin on the bacterial surface occurs preferentially along the sides of the bacterium, not at the poles. Biophysical models of stress produced during actin gel growth have shown that an actin gel becomes thicker when the geometry of the surface is less curved (17). This finding could explain the observed lateral actin accumulation along the sides of the bacterium, which are cylindrical, rather than at the poles, which are hemispherical. Experiments on ActA-coated vesicles have shown that much of the force generated by the actin gel during vesicle movement is compressive and is greatest along the sides of the vesicle (33,34). Aside from the highly curved hemispherical poles, the actin polymerization profile for bacteria during initiation correlates with the polar ActA distribution gradient along the long axis, with more actin accumulating near the rear, which has more ActA, than the front end. Thus the ActA density profile may localize compressive actin forces asymmetrically along the bacterium and result in the observed very slow initial movement forward before tail formation, where the compressive cloud squeezes the bacterium forward like a pinched watermelon seed.

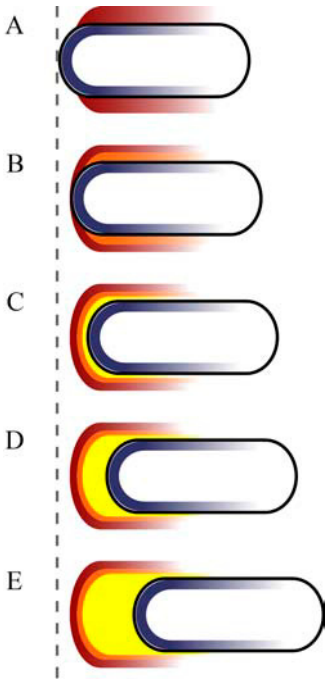

FIGURE 9 Model of the transition from initial actin accumulation to tail formation and movement. Black outline represents the bacterium. The polar ActA distribution on the surface is shown in blue. The actin that polymerized first (oldest actin) is shown in red, and the newest is in yellow. The dashed line indicates the stationary laboratory frame of reference. (*A*) Initial actin accumulation (*red*) occurs preferentially along the sides as the hemispherical poles have a disadvantage toward actin accumulation due to their greater curvature. (*B*) Side accumulation leads to slow forward movement, and a more rearward region of the bacterium is brought in contact with prepolymerized actin (*red*) remaining in the environment. New actin polymerizes (*orange*) along the sides but closer to the rear pole. (*C*) Further forward movement brings the pole itself into contact with older remaining actin (*red* and *orange*) stationary in the environment. The newest actin (*yellow*) is now able to accumulate rapidly at the pole due to autocatalytic actin nucleation and leads to polar cloud formation. (*D* and *E*) Repeated polar actin accumulation allows greater forward movement as the actin tail forms.

To understand the transition from initial actin accumulation to tail formation, there are two natural frames of reference to consider: the position of actin within the environment, which remains stationary (the laboratory or host cell frame of reference; see *dotted lin*e in Fig. 9), and the center of mass of the bacterium itself, which moves with respect to the environment (the bacterial frame of reference). The rate of F-actin accumulation at any point in space can be considered as a function of the local ActA density and surface curvature as well as of the density of preexisting, polymerized F-actin filaments, since dendritic actin network growth is autocatalytic (35,36). During initial actin accumulation, the hemispherical poles of the bacterium are at a disadvantage, due to their greater curvature, compared to the cylindrical sides (Fig. 9 *A*). When the bacterium begins to move forward slowly, through preferential lateral actin accumulation and the resultant compressive forces (Fig. 9 *B*), the

ActA density and bacterial curvature remain constant in the bacterial frame of reference. In contrast, the local density of F-actin, stationary in the environment, becomes dependent on bacterial movement history. With forward movement, the hemispherical poles of the bacterium are brought into contact with a local higher density of prepolymerized actin filaments that initially accumulated along the preferred sides and have remained stationary with respect to the environment (Fig. 9 *B*). The combination of increased ActA density at the pole and now increased F-actin as well overcomes the handicap of increased local curvature and allows dense polar actin growth. The repetitive process of new F-actin polymerization and bacterial translocation through the environment creates a differential actin amplification profile, which leads to the formation of the polar cloud (Fig. 9 *C*). At this point the greater polymerization at the pole may cause faster movement forward (Fig. 9 *D*), and polar actin growth and organization self-perpetuate as the actin tail forms (Fig. 9 *E*).

The gel-elastic models of actin accumulation and *L. monocytogenes* motility (17,37) can explain the preferential accumulation of actin along the cylindrical sides and the slow initial movement through compressive forces at those sides. The polar distribution of ActA provides the necessary asymmetry to localize the lateral forces to one end of the bacterium.

Experiments with flattened beads (disks) uniformly coated with ActA have shown that a curved surface is not required for steady-state movement (38). In these experiments, the most common configuration for stable motility was for disks to move by forming an actin tail on each side of the flattened surface. Although these results are consistent with our observations of preferential actin accumulation along the flat bacterial sides, these two disk-associated tails failed to convert into a single polarized structure. We propose that the hemispherical shape of the bacterial poles is necessary to allow the actin along the flat sides of bacteria to squeeze around the pole and be transformed into a coherent single actin tail.

Decrease in sensitivity as motility matures from initiation to steady state

The maturation process during motility initiation proceeds from a hopping regime to a persistent steady-state movement. The maturation of motility depends on bacterial movement, not on absolute length of exposure to cytoplasmic extract, as bacteria that initiate motility later still go through the full maturation process. The increased sensitivity to the environment during hopping early in initiation may lead to large variations among motility of different individuals due to even small differences in protein-protein interactions or ActA distribution. The high number of protein components and multicomponent interactions necessary for tail formation and motility (reviewed in Cameron et al. (12) and Pollard and Borisy (13)) most likely provides a new and distinct set of initial conditions each time bacterial motility is slowed and reinitiated.

One possible mechanism of motility maturation may be the increase in strength of the link between the bacterium and its actin tail. After the initial accumulation of a dense actin cloud around bacteria, the local surface density of actin drops dramatically due to the rapid speed as bacteria begin moving. Bacteria can no longer accumulate sufficient actin to perpetuate their motility and must therefore reaccumulate actin and repeatedly attempt initiating steady-state movement during the hopping regime. Hopping bacteria can be observed moving so rapidly that they lose their attachments to their actin tails. The observed relationship between actin density and speed are consistent with the explanation provided for hopping bacteria in the gel-elastic model of *L. monocytogenes* motility (37). Bacteria moving at steady state exhibit slower overall speeds and denser actin tails and can maintain their attachment to the actin tail. Thus the strength of the connection between the bacterium and the tail, which can be considered the frictional term in the gel-elastic model, must gradually increase during motility maturation. One way this could occur is through the slow accumulation of a molecular component, capable of increasing the frictional term, to the bacterial surface.

The structure and organization of the comet tail may also change during the maturation process. The organization of actin filaments within the stable comet tail includes highly branched shorter filaments within the center, surrounded by a sheath of bundled parallel actin filaments (39–41). The thickness and existence of this sheath varies among individual bacteria and extract preparations (41). Experiments with a partially reconstituted motility system have shown that actin filament organization during initial nucleation and elongation regulated by the Arp2/3 complex is that of short, cross-linked filaments associated with the rear pole of the bacterium. In contrast the elongation reaction in the absence of Arp2/3 results in bundles of filaments associated with the sides of the bacterium and is due to actin bundling proteins (41). This sheath of bundled actin could increase the persistence of motility by stiffening the comet tail, leading to more robust motility (39,41).

Discontinuous tails have been seen previously for bacteria expressing an ActA mutant deleting a portion of the N-terminal domain (42) now known to be important for interactions with actin and Arp2/3 (14). Additionally, members of the Ena/VASP protein family have recently been implicated in the formation of persistent comet tails. ActA-coated beads moving in a fully reconstituted system in the absence of VASP move with irregular speeds and discontinuous tails (31). The addition of pGolemi, a peptide that competes with ActA for binding to Ena/VASP proteins, to bacteria moving in extract leads to discontinuous tails at times in the initiation process when robust steady-state tails would otherwise have formed (32)), similar to our observations of motility for bacteria expressing the GRR ActA mutant. These results suggest

that the motility maturation process may involve functions of the Ena/VASP proteins, which have already been shown to contribute to other aspects of bacterial motility, include speed, and directional persistence (9–11). Ena/VASP proteins have further been shown both to affect the thickness and growth of actin gels (43) and to regulate filament organization within an actin network (44,45). Any of these functions could contribute to *L. monocytogenes* motility initiation and tail maturation.

Discontinuous tails have also been seen under other conditions. Beads coated with the VCA subdomain of the Wiscott-Aldrich syndrome protein (capable of activating Arp2/3), display hopping motility at steady state in a reconstituted system of purified proteins, and this hopping is dependant on the size of the bead (18). The hopping of VCA-coated beads, however, is distinct from the hopping regime observed for *L. monocytogenes* during motility initiation or in the presence of pGolemi, as the beads retain their actin tails persistently while hopping. VCA dependent movement occurs in the absence of VASP, which is implicated in the hopping regime of ActA dependent movement. Further, although hopping is just one regime an individual bacterium proceeds through during motility maturation, VCA-coated beads persist in a single regime during steady-state dependent on their size.

For *L. monocytogenes*, the transition from being stationary to moving seems to be universally sensitive to environmental conditions, whether within a host cell or in vitro. An obvious hopping regime was not seen for bacteria initiating motility within two different infected cell types. However, the cellular environment does not support motility of ActA-coated beads capable of moving within cytoplasmic extracts (19), indicating a different set of requirements in vivo for sufficient force generation to support unidirectional motility. The mechanism that allows for the transition from hopping to steady-state motility of bacteria in extract may be a prerequisite for bacterial motility within the cell.

Overall, the motility initiation process for *L. monocytogenes* is very complex and variable among individual bacteria and host cell environments and is affected by their nonspherical geometry, polarized and varying ActA distributions, and high sensitivity to the environment early in initiation. However, despite the immense variability apparent during initiation, the general bacterial geometry and protein distribution create a self-organized and renewing polymerizing actin structure that in all cases matures into the robust comet tail on the *L. monocytogenes* surface, with much lower variability in motility at the steady state (Fig. 1 *D* (20)). Widely varying initial conditions can greatly affect the initiation process but do not affect the final robust outcome. The increased complexity inherent to *L. monocytogenes* compared to simplified spherical artificial systems is thus crucial to their ability to overcome the significant challenges of initiating movement within the complex and variable physical environment of a host cell cytoplasm.

SUPPLEMENTARY MATERIAL

An online supplement to this article can be found by visiting BJ Online at http://www.biophysj.org.

We thank Fred Soo for help with the tracking program and Tanneke den Blaauwen for suggesting the linker sequence. We are grateful to Matt Footer for providing labeled actin, Pete Lauer, Dan Portnoy, and Roger Tsien for plasmids and strains, James Nelson for GFP-MDCKs, the Stanford FACS facility for their help in sorting PtK2 cells, and Peter Jackson for providing and housing *Xenopus laevis*. We also thank the Theriot lab for valuable and stimulating discussion, and Jonathan Alberts, Jiri Macas, Anne Meyer, Paula Soneral, Aaron Straight, and Cyrus Wilson for critical reading of the manuscript.

This work was supported by National Institutes of Health RO1 AI36929 and the American Heart Association. S.M.R. was supported by a National Science Foundation Predoctoral Fellowship.

REFERENCES

1. Lorber, B. 1997. Listeriosis. *Clin. Infect. Dis.* 24:1–9.
2. Bohne, J., Z. Sokolovic, and W. Goebel. 1994. Transcriptional regulation of prfA and PrfA-regulated virulence genes in Listeria monocytogenes. *Mol. Microbiol.* 11:1141–1150.
3. Freitag, N. E., and K. E. Jacobs. 1999. Examination of Listeria monocytogenes intracellular gene expression by using the green fluorescent protein of Aequorea victoria. *Infect. Immun.* 67:1844–1852.
4. Tilney, L. G., and D. A. Portnoy. 1989. Actin filaments and the growth, movement, and spread of the intracellular bacterial parasite, Listeria monocytogenes. *J. Cell Biol.* 109:1597–1608.
5. Kocks, C., R. Hellio, P. Gounon, H. Ohayon, and P. Cossart. 1993. Polarized distribution of Listeria monocytogenes surface protein ActA at the site of directional actin assembly. *J. Cell Sci.* 105:699–710.
6. Smith, G. A., D. A. Portnoy, and J. A. Theriot. 1995. Asymmetric distribution of the Listeria monocytogenes ActA protein is required and sufficient to direct actin-based motility. *Mol. Microbiol.* 17:945–951.
7. Welch, M. D., A. Iwamatsu, and T. J. Mitchison. 1997. Actin polymerization is induced by Arp2/3 protein complex at the surface of Listeria monocytogenes. *Nature.* 385:265–269.
8. Welch, M. D., J. Rosenblatt, J. Skoble, D. A. Portnoy, and T. J. Mitchison. 1998. Interaction of human Arp2/3 complex and the Listeria monocytogenes ActA protein in actin filament nucleation. *Science.* 281:105–108.
9. Smith, G. A., J. A. Theriot, and D. A. Portnoy. 1996. The tandem repeat domain in the Listeria monocytogenes ActA protein controls the rate of actin-based motility, the percentage of moving bacteria, and the localization of vasodilator-stimulated phosphoprotein and profilin. *J. Cell Biol.* 135:647–660.
10. Geese, M., J. J. Loureiro, J. E. Bear, J. Wehland, F. B. Gertler, and A. S. Sechi. 2002. Contribution of Ena/VASP proteins to intracellular motility of Listeria requires phosphorylation and proline-rich core but not F-actin binding or multimerization. *Mol. Biol. Cell.* 13:2383–2396.
11. Auerbuch, V., J. J. Loureiro, F. B. Gertler, J. A. Theriot, and D. A. Portnoy. 2003. Ena/VASP proteins contribute to Listeria monocytogenes pathogenesis by controlling temporal and spatial persistence of bacterial actin-based motility. *Mol. Microbiol.* 49:1361–1375.
12. Cameron, L. A., P. A. Giardini, F. S. Soo, and J. A. Theriot. 2000. Secrets of actin-based motility revealed by a bacterial pathogen. *Nat. Rev. Mol. Cell Biol.* 1:110–119.
13. Pollard, T. D., and G. G. Borisy. 2003. Cellular motility driven by assembly and disassembly of actin filaments. *Cell.* 112:453–465.
14. Lauer, P., J. A. Theriot, J. Skoble, M. D. Welch, and D. A. Portnoy. 2001. Systematic mutational analysis of the amino-terminal domain of

the Listeria monocytogenes ActA protein reveals novel functions in actin-based motility. *Mol. Microbiol.* 42:1163–1177.

15. Cameron, L. A., M. J. Footer, A. van Oudenaarden, and J. A. Theriot. 1999. Motility of ActA protein-coated microspheres driven by actin polymerization. *Proc. Natl. Acad. Sci. USA.* 96:4908–4913.
16. van Oudenaarden, A., and J. A. Theriot. 1999. Cooperative symmetry-breaking by actin polymerization in a model for cell motility. *Nat. Cell Biol.* 1:493–499.
17. Noireaux, V., R. M. Golsteyn, E. Friederich, J. Prost, C. Antony, D. Louvard, and C. Sykes. 2000. Growing an actin gel on spherical surfaces. *Biophys. J.* 78:1643–1654.
18. Bernheim-Groswasser, A., S. Wiesner, R. M. Golsteyn, M. F. Carlier, and C. Sykes. 2002. The dynamics of actin-based motility depend on surface parameters. *Nature.* 417:308–311.
19. Cameron, L. A., J. R. Robbins, M. J. Footer, and J. A. Theriot. 2004. Biophysical parameters influence actin-based movement, trajectory and initiation in a cell-free system. *Mol Biol Cell.* 15:2312–2323.
20. Soo, F. S., and J. A. Theriot. 2005. Large-scale analysis of sources of variation in the actin polymerization-based movement of *Listeria* monocytogenes. *Biophys. J.* In press.
21. Campbell, R. E., O. Tour, A. E. Palmer, P. A. Steinbach, G. S. Baird, D. A. Zacharias, and R. Y. Tsien. 2002. A monomeric red fluorescent protein. *Proc. Natl. Acad. Sci. USA.* 99:7877–7882.
22. Lauer, P., M. Y. Chow, M. J. Loessner, D. A. Portnoy, and R. Calendar. 2002. Construction, characterization, and use of two Listeria monocytogenes site-specific phage integration vectors. *J. Bacteriol.* 184:4177–4186.
23. Grundling, A., M. D. Gonzalez, and D. E. Higgins. 2003. Requirement of the Listeria monocytogenes broad-range phospholipase PC-PLC during infection of human epithelial cells. *J. Bacteriol.* 185:6295–6307.
24. Robbins, J. R., A. I. Barth, H. Marquis, E. L. de Hostos, W. J. Nelson, and J. A. Theriot. 1999. Listeria monocytogenes exploits normal host cell processes to spread from cell to cell. *J. Cell Biol.* 146:1333–1350.
25. Skoble, J., V. Auerbuch, E. D. Goley, M. D. Welch, and D. A. Portnoy. 2001. Pivotal role of VASP in Arp2/3 complex-mediated actin nucleation, actin branch-formation, and Listeria monocytogenes motility. *J. Cell Biol.* 155:89–100.
26. Theriot, J. A., and D. C. Fung. 1997. Use of *Xenopus* egg extracts for studies of actin-based motility. *In* Cell Biology: A Laboratory Handbook. J. E. Celis, editor. Academic Press, New York. 350–358.
27. Pardee, J. D., and J. A. Spudich. 1982. Purification of muscle actin. *Methods Enzymol.* 85(Pt. B):164–181.
28. Murray, A. W. 1991. Cell cycle extracts. *Methods Cell Biol.* 36:581–605.
29. Lacayo, C. I., and J. A. Theriot. 2004. Listeria monocytogenes actin-based motility varies depending on subcellular location: a kinematic probe for cytoarchitecture. *Mol. Biol. Cell.* 15:2164–2175.
30. Kocks, C., and P. Cossart. 1993. Directional actin assembly by Listeria monocytogenes at the site of polar surface expression of the actA gene product involving the actin-bundling protein plastin (fimbrin). *Infect. Agents Dis.* 2:207–209.
31. Samarin, S., S. Romero, C. Kocks, D. Didry, D. Pantaloni, and M. F. Carlier. 2003. How VASP enhances actin-based motility. *J. Cell Biol.* 163:131–142.
32. Golemi-Kotra, D., R. Mahaffy, M. J. Footer, J. H. Holtzman, T. D. Pollard, J. A. Theriot, and A. Schepartz. 2004. High affinity, paralog-specific recognition of the Mena EVH1 domain by a miniature protein. *J. Am. Chem. Soc.* 126:4–5.
33. Giardini, P. A., D. A. Fletcher, and J. A. Theriot. 2003. Compression forces generated by actin comet tails on lipid vesicles. *Proc. Natl. Acad. Sci. USA.* 100:6493–6498.
34. Upadhyaya, A., and A. van Oudenaarden. 2003. Biomimetic systems for studying actin-based motility. *Curr. Biol.* 13:R734–R744.
35. Higgs, H. N., L. Blanchoin, and T. D. Pollard. 1999. Influence of the C terminus of Wiskott-Aldrich syndrome protein (WASp) and the Arp2/3 complex on actin polymerization. *Biochemistry.* 38:15212–15222.
36. Machesky, L. M., R. D. Mullins, H. N. Higgs, D. A. Kaiser, L. Blanchoin, R. C. May, M. E. Hall, and T. D. Pollard. 1999. Scar, a WASp-related protein, activates nucleation of actin filaments by the Arp2/3 complex. *Proc. Natl. Acad. Sci. USA.* 96:3739–3744.
37. Gerbal, F., P. Chaikin, Y. Rabin, and J. Prost. 2000. An elastic analysis of Listeria monocytogenes propulsion. *Biophys. J.* 79:2259–2275.
38. Schwartz, I. M., M. Ehrenberg, M. Bindschadler, and J. L. McGrath. 2004. The role of substrate curvature in actin-based pushing forces. *Curr. Biol.* 14:1094–1098.
39. Zhukarev, V., F. Ashton, J. M. Sanger, J. W. Sanger, and H. Shuman. 1995. Organization and structure of actin filament bundles in Listeria-infected cells. *Cell Motil. Cytoskeleton.* 30:229–246.
40. Sechi, A. S., J. Wehland, and J. V. Small. 1997. The isolated comet tail pseudopodium of Listeria monocytogenes: a tail of two actin filament populations, long and axial and short and random. *J. Cell Biol.* 137: 155–167.
41. Brieher, W. M., M. Coughlin, and T. J. Mitchison. 2004. Fascin-mediated propulsion of Listeria monocytogenes independent of frequent nucleation by the Arp2/3 complex. *J. Cell Biol.* 165:233–242.
42. Lasa, I., E. Gouin, M. Goethals, K. Vancompernolle, V. David, J. Vandekerckhove, and P. Cossart. 1997. Identification of two regions in the N-terminal domain of ActA involved in the actin comet tail formation by Listeria monocytogenes. *EMBO J.* 16:1531–1540.
43. Plastino, J., S. Olivier, and C. Sykes. 2004. Actin filaments align into hollow comets for rapid VASP-mediated propulsion. *Curr. Biol.* 14: 1766–1771.
44. Bear, J. E., T. M. Svitkina, M. Krause, D. A. Schafer, J. J. Loureiro, G. A. Strasser, I. V. Maly, O. Y. Chaga, J. A. Cooper, G. G. Borisy, and F. B. Gertler. 2002. Antagonism between Ena/VASP proteins and actin filament capping regulates fibroblast motility. *Cell.* 109:509–521.
45. Plastino, J., I. Lelidis, J. Prost, and C. Sykes. 2004. The effect of diffusion, depolymerization and nucleation promoting factors on actin gel growth. *Eur. Biophys. J.* 33:310–320.
46. Ambrose, H. W., and K. P. Ambrose. 1987. A Handbook of Biological Investigation. Hunter Textbooks, Knoxville, TN.